

Orthorhombic charge density wave on the tetragonal lattice of EuAl_4

SITARAM RAMAKRISHNAN,^{a,b*} SURYA ROHITH KOTLA,^a TOMS REKIS,^a
 JIN-KE BAO,^{a,c} CLAUDIO EISELE,^a LEILA NOOHINEJAD,^d MARTIN TOLKIEHN,^d
 CARSTEN PAULMANN,^{d,e} BIRENDER SINGH,^f RAHUL VERMA,^f BIPLAB BAG,^f
 RUTA KULKARNI,^f ARUMUGAM THAMIZHAVEL,^f BAHADUR SINGH,^{f*}
 SRINIVASAN RAMAKRISHNAN^{f*} AND SANDER VAN SMAALEN^{a*}

^a*Laboratory of Crystallography, University of Bayreuth, 95447 Bayreuth Germany,*

^b*Department of Quantum Matter, AdSM, Hiroshima University, 739-8530,
 Higashi-Hiroshima Japan,* ^c*Department of Physics, Materials Genome Institute and
 International Center for Quantum and Molecular Structures, Shanghai University,*

Shanghai 200444, P. R. China, ^d*P24, PETRA III, Deutsches
 Elektronen-Synchrotron DESY, Notkestr. 85, 22607 Hamburg Germany,*

^e*Mineralogisch-Petrographisches Institut, Universität Hamburg, 20146 Hamburg
 Germany,* and ^f*Department of Condensed Matter Physics and Materials
 Science, Tata Institute of Fundamental Research, Mumbai 400005 India.*

*E-mail: niranj002@gmail.com, bahadur.singh@tifr.res.in, ramky07@gmail.com,
 smash@uni-bayreuth.de*

Charge density wave, Twinning, Modulated, Superspace

Abstract

EuAl₄ possesses the BaAl₄ crystal structure type with tetragonal symmetry $I4/mmm$. It undergoes a charge-density-wave (CDW) transition at $T_{CDW} = 145$ K and it features four consecutive antiferromagnetic phase transitions below 16 K. Here, we use single-crystal x-ray diffraction to determine incommensurately modulated crystal structure of EuAl₄ in its CDW state. The CDW is shown to be incommensurate with modulation wave vector $\mathbf{q} = (0, 0, 0.1781(3))$ at 70 K. The symmetry of the incommensurately modulated crystal structure is orthorhombic with superspace group $Fmmm(00\sigma)s00$, where $Fmmm$ is a subgroup of $I4/mmm$ of index 2. Both the lattice and the atomic coordinates of the basic structure remain tetragonal. Symmetry breaking is entirely due to the modulation wave, where atoms Eu and Al1 have displacements exclusively along \mathbf{a} , while the fourfold rotation would require equal displacement amplitudes along \mathbf{a} and \mathbf{b} . The calculated band structure of the basic structure and interatomic distances in the modulated crystal structure both indicate the aluminum atoms as location of the CDW. The temperature dependence of the specific heat reveals an anomaly at $T_{CDW} = 145$ K of a magnitude similar to canonical CDW systems. The present discovery of orthorhombic symmetry for the CDW state of EuAl₄ leads to the suggestion of monoclinic instead of orthorhombic symmetry for the third AFM state.

1. Introduction

EuAl₄ has attracted attention, because it develops a charge-density wave (CDW) below $T_{CDW} = 145.1$ K and it exhibits four successive magnetic transitions below 16 K (Nakamura *et al.*, 2015; Shimomura *et al.*, 2019). EuAl₄ adopts the BaAl₄ structure type that has symmetry according to the tetragonal space group $I4/mmm$ (Parthé *et al.*, 1983; Nakamura *et al.*, 2015), as shown in Fig. 1. It belongs to a large family of isostructural compounds, including magnetic EuGa₄, fully ordered EuAl₂Ga₂ and

non-magnetic SrAl₄ and BaAl₄ (Nakamura *et al.*, 2016; Stavinoha *et al.*, 2018; Ōnuki *et al.*, 2020). Recently, a symmetry-protected non-trivial topology of the electronic band structure was proposed for BaAl₄ (Wang *et al.*, 2021). In case of magnetic EuAl₄, a chiral spin structure, like skyrmions reported in some divalent Eu compounds such as EuPtSi (Kaneko *et al.*, 2019; Ōnuki *et al.*, 2020), was proposed on the basis of the observation of the topological Hall resistivity and muon-spin rotation and relaxation (μ SR) studies (Shang *et al.*, 2021; Zhu *et al.*, 2022). If such a nontrivial texture would be confirmed, EuAl₄ would represent a rare case of a compound where one could observe the coexistence of exotic magnetic order and a CDW. Since these exotic electronic and spin structures depend on the symmetry, knowledge of the true symmetry of the crystal structure thus is of utmost importance for understanding non-trivial magnetic properties. Here we show that the CDW transition of EuAl₄ is accompanied by a lowering of the symmetry towards orthorhombic, and we present the incommensurately modulated CDW crystal structure.

EuAl₄ is one of a few compounds (Schutte *et al.*, 1993), where the lowering of the crystal symmetry at a phase transition is governed by the symmetry of the incommensurate modulation wave describing the CDW, while any lattice distortion could not be detected in the present high-resolution diffraction experiment with synchrotron radiation. This feature might explain why the lowering of symmetry has not been found in earlier studies on EuAl₄. This behavior is in contrast to other CDW materials, like Er₂Ir₃Si₅, Lu₂Ir₃Si₅ and BaFe₂Al₉, for which the CDW transitions are accompanied by large lattice distortions (Ramakrishnan *et al.*, 2020; Ramakrishnan *et al.*, 2021; Meier *et al.*, 2021)

The phenomenon of CDW was originally identified as a property of crystals with quasi-one-dimensional (1D) electron bands, such as NbSe₃ and K_{0.3}MoO₃ (Gruner, 1994; Monceau, 2012). A CDW is formed due to Fermi surface nesting (FSN), where

the nesting vector of the periodic structure becomes the wave vector of the CDW of the metallic bands as well as of the accompanying modulation of the atomic positions (periodic lattice distortion—PLD). The modulation wave vector can be commensurate or incommensurate with respect to the underlying periodic basic structure. More recent research has found that CDWs can develop in crystalline materials that lack the 1D property of their crystal structures and rather possess three-dimensionally (3D) structured electron bands. Alternate mechanisms have been proposed for the formation of CDWs in 3D compounds, including the mechanism of q -dependent electron-phonon coupling (EPC) (Zhu *et al.*, 2015; Zhu *et al.*, 2017). Strongly correlated electron systems may also support the formation of CDWs (Chen *et al.*, 2016). The latter are often found for rare-earth containing intermetallic compounds, like the series of isostructural compounds $R_5\text{Ir}_4\text{Si}_{10}$ ($R = \text{rare earth}$) (Ramakrishnan & van Smaalen, 2017).

The interplay between CDWs and magnetism in rare-earth compounds continues to attract attention. A competition between these two symmetry-breaking phenomena can be expected, because both CDWs and magnetic order depend on the Fermi surface through FSN and the Ruderman-Kittel-Kasuya-Yosida (RKKY) interaction between the localized magnetic moments of the $4f$ electrons, as it is found for EuAl_4 (Kobata *et al.*, 2016). In case of magnetoelastic coupling, the lattice distortion may couple to the PLD or the lattice distortion in the CDW state or to the EPC. Experimentally, the coexistence of a CDW and antiferromagnetic (AFM) order has been established for $\text{Er}_5\text{Ir}_4\text{Si}_{10}$ and $\text{Sm}_2\text{Ru}_3\text{Ge}_5$ (Galli *et al.*, 2002; Kuo *et al.*, 2020). The series of compounds $R\text{NiC}_2$ ($R = \text{Pr, Nd, Gd, Tb, Dy, Ho, Er}$) exhibit both CDW and AFM phase transitions (Roman *et al.*, 2018; Shimomura *et al.*, 2016; Kolincio *et al.*, 2017; Maeda *et al.*, 2019). SmNiC_2 is an exception in this series, since it develops ferromagnetic (FM) order below $T_C = 17.7$ K at which transition the CDW is destroyed (Shimomura *et al.*, 2009; Wölfel *et al.*, 2010). Recently, coexistence of CDW and FM orders was

found for the field-induced FM state of TmNiC_2 (Kolincio *et al.*, 2020).

Magnetism of EuAl_4 is related to localized magnetic moments of the europium atoms in their divalent state: the electronic configuration $4f^7$ implies $J = S = 7/2$ and $L = 0$, where J is the total angular momentum, S is the spin angular momentum and L is the orbital angular momentum (Wernick *et al.*, 1967; Nakamura *et al.*, 2015). This allows the study of the collective magnetism without single-ion anisotropy, as divalent Eu has zero orbital angular momentum. Magnetic interactions are governed by the RKKY interaction (Nakamura *et al.*, 2015). Neutron diffraction has established that the AFM order involves an incommensurate modulation wave (Kaneko *et al.*, 2021). Single-crystal x-ray diffraction (SXRD) has shown the coexistence of the incommensurate CDW modulation and AFM order (Shimomura *et al.*, 2019). Furthermore, Shimomura *et al.* (2019) proposed a lowering of the lattice symmetry at the third magnetic transition towards $Immm$ orthorhombic. This is essentially different from the present discovery of $Fmmm$ orthorhombic symmetry below the CDW transition.

EuAl_4 possesses a 3D band structure with localized $4f$ electrons of Eu well below the Fermi surface (Kobata *et al.*, 2016). The CDW mainly involves orbitals of the Al atoms (Kaneko *et al.*, 2021). This is in agreement with the observation of a CDW with $T_{CDW} = 243$ K in isostructural SrAl_4 , where non-magnetic Sr replaces Eu (Nakamura *et al.*, 2016; Niki *et al.*, 2020). Here we present electronic band-structure calculations for the tetragonal structure of EuAl_4 . They confirm that the location of the CDW is on the Al atoms. They reveal a 3D band structure with a highly structured Fermi surface.

2. Experimental and Computational details

Single-crystals of EuAl_4 were synthesized by the Al self-flux method. The elements europium (Lieco, 99.9% purity) and aluminum (Alfa Aesar, 99.999%) were filled into an alumina crucible in the ratio 1:20. The crucible was sealed in an evacuated quartz glass ampoule. It was heated to a temperature of 1323 K and held at this temperature for 24 hours. After which the crucible was cooled down to 1073 K in 6 hours and then slowly cooled at a rate of 2 K/hr down to 923 K at which point the crystals were separated from the molten metal by centrifugation. The 1:4 stoichiometry of the product was confirmed by energy-dispersive x-ray spectroscopy (EDX) as well as by the structure refinements against SXR D data.

X-ray diffraction experiments were performed at Beamline P24 of PETRA-III at DESY in Hamburg, employing radiation of a wavelength of 0.5000 Å. The temperature of the specimen was controlled by a CRYOCOOL open-flow helium gas cryostat. Complete data sets of intensities of Bragg reflections were measured at temperatures of 250 K (tetragonal phase), and of 70 K and 20 K (CDW phase). Each run of data collection comprises 3640 frames, corresponding to a rotation of the crystal over 364 deg, which was repeated 10 times. These data were binned to a data set of 364 frames of 1 deg of rotation and 10 seconds exposure time, using the SNBL toolbox (Dyadkin *et al.*, 2016). See Section S1 in the supporting information.

The EVAL15 software suite (Schreurs *et al.*, 2010) has been used for processing the SXR D data. At 250 K a single run was collected at a crystal-to-detector distance of at 110 mm and without a 2θ offset of the detector. At 70 K and at 20 K a crystal-to-detector distance of 260 mm required two runs, with and without 2θ offset, respectively. The two binned runs for 70 K and those for 20 K were integrated separately, and subsequently merged in the module ANY of EVAL15. SADABS (Sheldrick, 2008) has been used for scaling and absorption correction with Laue symmetry $4/mmm$

for the 250 K data and mmm for 70 K and 20 K. The reflection file produced was imported to Jana2006 (Petricek *et al.*, 2014; Petricek *et al.*, 2016). Table 1 shows the crystallographic information.

The magnetic susceptibility $\chi(T)$ has been measured for temperatures 2.5–300 K, using a commercial SQUID magnetometer (MPMS5 by Quantum Design, USA). Measurements have been made in fields of 0.1 T and 0.5 T.

The specific heat, $C_p(T)$, has been measured from 220 to 8 K by the thermal relaxation method, using a physical property measuring system (PPMS, Quantum Design, USA).

Density functional theory (DFT) based calculations were performed within the generalized gradient approximation (GGA) using the projector augmented (PAW) wave method as implemented in the Vienna *Ab-initio* Simulation Package (VASP) (Kresse & Joubert, 1999; Kresse & Furthmüller, 1996). The Perdew-Burke-Ernzerhof (PBE) functional was used to consider the exchange-correlation effects (Perdew *et al.*, 1996). An energy cutoff of 380 eV was used for the plane-wave basis set, and a Γ -centered, $9 \times 9 \times 9$ k mesh was employed for the bulk Brillouin zone sampling. Spin-orbit coupling effects were considered in all the calculations. We employed Eu^{2+} by considering the remaining $4f$ electrons as core electrons. A tight-binding Hamiltonian was generated to compute the Fermi surface on a finer k grid (Marzari & Vanderbilt, 1997). The FermiSurfer software package was used to visualize the Fermi surface (Kawamura, 2019).

3. Discussion

3.1. Analysis of the CDW structure

SXRD at 250 K confirmed the $I4/mmm$ crystal structure of EuAl_4 . The SXRD data at 70 K revealed satellite reflections at positions that can be described by the modulation wave vector $\mathbf{q} = (0, 0, 0.1781(3))$, in agreement with the results by Naka-

mura *et al.* (2015) and Shimomura *et al.* (2019). Visualisation of the SXR D data was done with aid of the software CrysAlisPRO (Rigaku, 2019). Figs. 2(a) and 2(b) show a small part of the $(0, k, l)$ plane of the reconstructed reciprocal lattice. Satellite reflections along \mathbf{c}^* are clearly visible at 70 K [Fig. 2(b)]. Upon further cooling to 20 K, there is a reduction by 0.004 in the σ_3 component of the modulation wave vector, in agreement with Shimomura *et al.* (2019).

We note that the lattice parameters in the CDW phase do not give evidence for an orthorhombic lattice distortion. This could explain why earlier works have not found this symmetry lowering.

In order to determine the crystal structure of the CDW phase, we have tested different superspace groups for its symmetry (See Table S2 in the supporting information). It is noticed that the tetragonal lattice allows two fundamentally different orthorhombic lattices as subgroups: $Immm$ preserves the mirror planes perpendicular to the \mathbf{a} and \mathbf{b} axes of $I4/mmm$, while $Fmmm$ preserves the diagonal mirror planes. Table 2 provides the crystallographic data for three of the refined crystal structures (compare Table S2 in the supporting information). The three models, A, B and C, are discussed below.

3.1.1. Model A: In the diffraction pattern we did not observe any splitting of the main or satellite reflections, where split reflections would indicate a twinned crystal of lower symmetry. Also, we did not find a distortion in the lattice parameters, as it would occur for a single-domain crystal of lower symmetry. Furthermore, the preservation of tetragonal symmetry within the CDW phase was reported in the literature (Nakamura *et al.*, 2015; Shimomura *et al.*, 2019). Therefore, initial data processing was performed under the assumption of tetragonal symmetry, employing point group $4/mmm$ for scaling and absorption correction in SADABS (Sheldrick, 2008)). Struc-

ture refinements of the incommensurately modulated structure were performed with a model with superspace group $I4/mmm(00\sigma)0000$. Table 2 shows that R_{int} as well as R_F for the main reflections are reasonably low, indicating that the average structure of the CDW phase still is tetragonal in good approximation. This conclusion is reinforced by the fact that refinement of the average structure against main reflections leads to $R_F = 1.55\%$; an excellent fit. However, $R_F = 60.46\%$ for the satellite reflections. This high value indicates that the satellite reflections are not well fitted and that the CDW modulation does not have tetragonal symmetry.

This makes Model A an unsuitable candidate for the incommensurate CDW structure. Other tetragonal superspace groups were also tested, leading to similar failures in describing the modulation wave or with reflection conditions violated by the measured SXRD data (see Table S2 in the supporting information). As a result we can rule out tetragonal symmetry for the modulated CDW crystal structure.

3.1.2. Model B: As second model we have considered a lowering of the symmetry from tetragonal $I4/mmm$ to its orthorhombic subgroup $Immm$. This orthorhombic point symmetry was used for scaling and absorption correction of the SXRD data in SADABS (Sheldrick, 2008)). The CDW phase transition allows for pseudomerohedral twinning of two, differently oriented domains on the tetragonal lattice, that are related by the missing fourfold rotation (Parsons, 2003). Since split reflections or a lattice distortion could not be detected in the SXRD data, all Bragg reflections have contributions from both domains. The structure refinement of a model in superspace group $Immm(00\sigma)s00$ has lead to a twin volume ratio of 0.485 : 0.515, thus explaining the nearly tetragonal point symmetry of the SXRD data. R -values indicate a good fit to the SXRD data for this model (Table 2). As a result, this model is a prime candidate for describing the incommensurately modulated crystal structure of the CDW

phase.

3.1.3. Model C: As last model we present model C with symmetry according to $Fmmm$, the other orthorhombic subgroup, which now preserves the diagonal mirror planes of $I4/mmm$. Scaling and absorption correction of the SXRD data was performed with SADABS according to the differently oriented point group mmm (Sheldrick, 2008). Again, two domains are possible that are related by the missing four-fold rotation. The structure refinement of a model in superspace group $Fmmm(00\sigma)s00$ has lead to a twin volume ratio of 0.454(4) : 0.546, thus explaining the nearly tetragonal point symmetry of the SXRD data. R -values indicate an excellent fit to the SXRD data for this model (Table 2), which is significantly better than that of model B. Furthermore, the refined parameters possess slightly smaller s.u.'s in model C than in model B, while the number of parameters is one smaller in model C (Tables S3 and S4 in the supporting information). Therefore, the best fit to the SXRD data has been obtained for a modulated crystal structure with symmetry according to the superspace group $Fmmm(00\sigma)s00$. $Fmmm(00\sigma)0s0$ is an alternate setting of this superspace group, while all other symmetries lead to a worse fit to the SXRD data (Table S2 in the supporting information).

Recently, Kaneko *et al.* (2021) have proposed that the CDW of EuAl_4 involves displacements of the Al atoms perpendicular to \mathbf{c} , while Eu would not be involved in the PLD. The present crystal structure involves atomic modulations exclusively perpendicular to \mathbf{c} , as it is enforced by the superspace symmetry (Table S4). However, the modulation amplitudes are of comparable magnitude for all three atoms, Eu, Al1 and Al2. Nevertheless, a non-zero modulation amplitude is not evidence by itself, that the involved atom must contribute electronic states to the CDW. The atomic modulation may also be caused by the elastic coupling to other atoms that are carrying

the CDW. In EuAl_4 , the shortest interatomic distances are between Al2 atoms and for Al1–Al2 [Fig. 3(a)]. They are hardly modulated, and forming a two-dimensional network of Al perpendicular to \mathbf{c} (Fig. 1). The largest modulation is found for the next shorter Al–Al distance between Al1 atoms [Fig. 3(b)]. This strong modulation suggests that the CDW resides on the layers of Al atoms. Eu is elastically coupled to Al1 and Al2 (Fig. S1) and is not part of the CDW. The t plots of interatomic distances cannot elaborate on the precise location: the CDW resides either on the Al1 atoms or on a network of Al1 and Al2 atoms (Fig. 3).

3.2. Electronic structure and Fermi surface

Figure 4(a) shows the calculated band structure along the high-symmetry directions in the primitive Brillouin zone of the periodic crystal structure of EuAl_4 with $I4/mmm$ symmetry. Both the valence and conduction bands cross the Fermi level E_F , resolving its metallic ground state. Importantly, the bands along Γ – Z have a substantial energy dispersion. This indicates the three-dimensional nature of the Fermi surface as discussed below. There is a Dirac nodal crossing above the Fermi level along the Γ – Z direction, which is protected by C_{4z} rotational symmetry. EuAl_4 thus realizes a Dirac semimetallic state. To resolve the electronic states near E_F , we present the atom-projected density of states (PDOS) in Fig. 4(b); Eu PDOS is in blue and Al PDOS is in red. The Al states are dominant at E_F , indicating that Al atoms are predominantly metallic and more likely undergo CDW modulations, in agreement with the analysis of PLD (Section 3.1) and the literature. PDOS of Eu comprises of d states at the Fermi level, while $4f$ states are well below E_F , in agreement with the literature (Kobata *et al.*, 2016).

We present the calculated Fermi pockets associated with the valence (h^+) and conduction states (e^-) in Figs. 4(c,d). They reveal a hole pocket centered on Γ and an

electron Fermi pocket centered on Z . Both Fermi pockets are highly structured. The e^- Fermi pocket suggest the possibility of nesting perpendicular to the \mathbf{c} axes. For the h^+ pocket a possible FSN is not clearly resolved. It should however be noted that because of the 3D nature of the Fermi surface, the nesting may have a complicated structure. These results do not clearly indicate FSN as mechanism for the formation of the CDW state in EuAl_4 .

3.3. Magnetic susceptibility

The temperature dependence of the magnetic susceptibility, measured with magnetic fields of 0.1 T and 0.5 T, is shown for 2.4–300 K in Fig. 5. Any change of the susceptibility at the CDW transition (*e.g.* as a change of Pauli paramagnetism) is masked by the large value of the paramagnetic susceptibility. However, the low temperature data reveal an AFM transition below 16 K, which agrees with the previously published value (Nakamura *et al.*, 2015).

3.4. Specific heat

The temperature dependence of the specific heat (C_p) is shown for 8–210 K in Fig. 6. The high temperature data clearly reveal a small, broad jump of $\Delta C_p = 2.5 \text{ J}/(\text{mol K})$ at 145 K, suggesting a thermodynamic phase transition (CDW) at 145 K. Such an anomaly in the temperature dependence of the specific heat is consistent with that observed in canonical CDW systems, like NbSe_3 (Tomić *et al.*, 1981). The low-temperature data display multiple AFM transitions, which have also been observed in earlier studies (Nakamura *et al.*, 2015).

4. Conclusions

EuAl₄ possesses the BaAl₄ crystal structure type with tetragonal symmetry $I4/mmm$. It undergoes a CDW transition at $T_{CDW} = 145$ K. Here, we have presented the incommensurately modulated crystal structure of EuAl₄ in its CDW state. Structure refinements according to the superspace approach have shown that: (i) the modulation is incommensurate with modulation wave vector $\mathbf{q} = (0, 0, 0.1781(3))$ at 70 K, in agreement with Shimomura *et al.* (2019); and (ii) the symmetry of the CDW crystal structure is orthorhombic with superspace group $Fmmm(00\sigma)s00$, where $Fmmm$ is a subgroup of $I4/mmm$ of index 2. Despite this group–subgroup relation, we did not find any lattice distortion in the SXRD data. Even more, atomic positions of the basic structure of $Fmmm(00\sigma)s00$ still obey the $I4/mmm$ symmetry (Table S3). Symmetry breaking is entirely in the modulation wave (CDW and PLD), where atoms Eu and Al1 have displacements exclusively along \mathbf{a} of the F -centered unit cell (Table S4), while the fourfold rotation would require equal displacement amplitudes along \mathbf{a} and \mathbf{b} .

One interesting question is the location of the CDW. Analysis of the modulation of interatomic distances (Section 3.1) as well as features of the electronic band structure (Section 3.2) have indicated the Al atoms as supporting the CDW, in agreement with the literature (Kobata *et al.*, 2016; Kaneko *et al.*, 2021).

Compounds of rare earth (R) and transition metals, like $R_5\text{Ir}_4\text{Si}_{10}$ and $R_2\text{Ir}_3\text{Si}_5$, contain highly correlated electron systems, with accompanying influence on the mechanism of formation of CDWs. In EuAl₄, the majority element is the light p -block metal aluminum. Band-structure calculations have shown that FSN is a possible mechanism of CDW formation. Furthermore, the weak anomaly in $C_p(T)$ near T_{CDW} is similar to anomalies of canonical CDW materials and it is much smaller than observed for the rare-earth–transition-metal base compounds, again this would support the FSN mech-

anism. An alternative possibility is that the CDW is related to nesting of nontrivial bands that are present in the band structure (Shi *et al.*, 2021; Chiu *et al.*, 2022).

The present discovery of orthorhombic symmetry for the CDW state of EuAl_4 is important for modeling of the electronic properties of the CDW state as well as for identifying the correct magnetic order and understanding the magnetic properties of the four AFM states below 16 K.

Recent work either has used tetragonal symmetry for analysing the AFM states (Shang *et al.*, 2021; Kaneko *et al.*, 2021). Alternatively, Shimomura *et al.* (2019) have proposed orthorhombic $Immm$ symmetry for the third AFM state. This orthorhombic subgroup incorporates the perpendicular mirror planes of $I4/mmm$, while presently found $Fmmm$ is based on the diagonal mirror planes of $I4/mmm$. On the other hand, Shimomura *et al.* (2019) report peak splitting in neutron diffraction into "three maxima." Together with the present observation of lowering of symmetry at the CDW transition, this suggests that the third AFM state could have monoclinic symmetry (c unique) instead of orthorhombic symmetry, since, apparently, both the diagonal and perpendicular mirror planes are lost.

Acknowledgements We acknowledge DESY (Hamburg, Germany), a member of the Helmholtz Association HGF, for the provision of experimental facilities. Parts of this research were carried out at PETRA III, using beamline P24. Beamtime was allocated for proposal I-20190810. J.-K. Bao acknowledges the Alexander von Humboldt Foundation for financial support.

References

- Chen, C.-W., Choe, J. & Morosan, E. (2016). *Rep. Prog. Phys.* **79**(8), 084505.
- Chiu, W.-C., Chang, G., Macam, G., Belopolski, I., Huang, S.-M., Markiewicz, R., Yin, J.-X., Jia Cheng, Z., Lee, C.-C., Chang, T.-R., Chuang, F.-C., Xu, S.-Y., Lin, H., Hasan, M. Z. & Bansil, A. (2022). *ArXiv*; **2201.04757**.
- Dyadkin, V., Pattison, P., Dmitriev, V. & Chernyshov, D. (2016). *J. Synchrotron Rad.* **23**(3), 825–829.
- Galli, F., Feyerherm, R., Hendrikx, R. W. A., Dudzik, E., Nieuwenhuys, G. J., Ramakrishnan, S., Brown, S. D., van Smaalen, S. & Mydosh, J. A. (2002). *J. Phys.: Condens. Matter*, **14**, 5067–5075.

- Gruner, G. (1994). *Density waves in solids*. Reading, Massachusetts: Addison–Wesley.
- Kaneko, K., Frontzek, M. D., Matsuda, M., Nakao, A., Munakata, K., Ohhara, T., Kakihana, M., Haga, Y., Hedo, M., Nakama, T. & Onuki, Y. (2019). *J. Phys. Soc. Jpn.* **88**(1), 013702.
- Kaneko, K., Kawasaki, T., Nakamura, A., Munakata, K., Nakao, A., Hanashima, T., Kiyonagi, R., Ohhara, T., Hedo, M., Nakama, T. & Onuki, Y. (2021). *J. Phys. Soc. Jpn.* **90**(6), 064704.
- Kawamura, M. (2019). *Comput. Phys. Commun.* **239**, 197.
- Kobata, M., Fujimori, S.-i., Takeda, Y., Okane, T., Saitoh, Y., Kobayashi, K., Yamagami, H., Nakamura, A., Hedo, M., Nakama, T. & Onuki, Y. (2016). *J. Phys. Soc. Jpn.* **85**(9), 094703.
- Kolincio, K. K., Roman, M. & Klimczuk, T. (2020). *Phys. Rev. Lett.* **125**, 176601.
- Kolincio, K. K., Roman, M., Winiarski, M. J., Strychalska-Nowak, J. & Klimczuk, T. (2017). *Phys. Rev. B*, **95**(23), 235156.
- Kresse, G. & Furthmüller, J. (1996). *Phys. Rev. B*, **54**, 11169.
- Kresse, G. & Joubert, D. (1999). *Phys. Rev. B*, **59**, 1758.
- Kuo, C. N., Hsu, C. J., Tseng, C. W., Chen, W. T., Lin, S. Y., Liu, W. Z., Kuo, Y. K. & Lue, C. S. (2020). *Phys. Rev. B*, **101**, 155140.
- Maeda, H., Kondo, R. & Nogami, Y. (2019). *Phys. Rev. B*, **100**, 104107.
- Marzari, N. & Vanderbilt, D. (1997). *Phys. Rev. B*, **56**, 12847.
- Meier, W. R., Chakoumakos, B. C., Okamoto, S., McGuire, M. A., Hermann, R. P., Samolyuk, G. D., Gao, S., Zhang, Q., Stone, M. B., Christianson, A. D. & Sales, B. C. (2021). *Chem. Mater.* **33**, 2855–2863.
- Monceau, P. (2012). *Adv. Phys.* **61**(4), 325–581.
- Nakamura, A., Uejo, T., Harima, H., Araki, S., Kobayashi, T. C., Nakashima, M., Amako, Y., Hedo, M., Nakama, T. & Onuki, Y. (2016). *J. Alloys Compd.* **654**, 290–299.
- Nakamura, A., Uejo, T., Honda, F., Takeuchi, T., Harima, H., Yamamoto, E., Haga, Y., Matsubayashi, K., Uwatoko, Y., Hedo, M., Nakama, T. & Onuki, Y. (2015). *J. Phys. Soc. Jpn.* **84**(12), 124711.
- Niki, H., Kuroshima, H., Higa, N., Morishima, M., Yogi, M., Nakamura, A., Niki, K., Maehira, T., Hedo, M., Nakama, T. & Onuki, Y. (2020). *Proceedings of the International Conference on Strongly Correlated Electron Systems (SCES2019)*.
- Ōnuki, Y., Hedo, M. & Honda, F. (2020). *J. Phys. Soc. Jpn.* **89**(10), 102001.
- Parsons, S. (2003). *Acta Crystallogr. D*, **59**(11), 1995–2003.
- Parthé, E., Chabot, B., Braun, H. F. & Engel, N. (1983). *Acta Crystallogr. B*, **39**(5), 588–595.
- Perdew, J. P., Burke, K. & Ernzerhof, M. (1996). *Phys. Rev. Lett.* **77**, 3865.
- Petricek, V., Dusek, M. & Palatinus, L. (2014). *Z. Kristallogr.* **229**, 345–352.
- Petricek, V., Eigner, V., Dusek, M. & Cejchan, A. (2016). *Z. Kristallogr.* **231**(5), 301–312.
- Ramakrishnan, S., Schönleber, A., Bao, J.-K., Rekiş, T., Kotla, S. R., Schaller, A. M., van Smaalen, S., Noohinejad, L., Tolkiehn, M., Paulmann, C., Sangeetha, N. S., Pal, D., Thamizhavel, A. & Ramakrishnan, S. (2021). *Phys. Rev. B*, **104**, 054116.
- Ramakrishnan, S., Schönleber, A., Rekiş, T., van Well, N., Noohinejad, L., van Smaalen, S., Tolkiehn, M., Paulmann, C., Bag, B., Thamizhavel, A., Pal, D. & Ramakrishnan, S. (2020). *Phys. Rev. B*, **101**, 060101(R).
- Ramakrishnan, S. & van Smaalen, S. (2017). *Rep. Prog. Phys.* **80**, 116501.
- Rigaku, (2019). CrysAlis pro version 171.40.53, rigaku oxford diffraction.
- Roman, M., Strychalska-Nowak, J., Klimczuk, T. & Kolincio, K. K. (2018). *Phys. Rev. B*, **97**(4), 041103(R).
- Schreurs, A. M. M., Xian, X. & Kroon-Batenburg, L. M. J. (2010). *J. Appl. Crystallogr.* **43**, 70–82.
- Schutte, W. J., Disselborg, F. & de Boer, J. L. (1993). *Acta Crystallogr. B*, **49**, 787–794.

- Shang, T., Xu, Y., Gawryluk, D. J., Ma, J. Z., Shiroka, T., Shi, M. & Pomjakushina, E. (2021). *Phys. Rev. B*, **103**, L020405.
- Sheldrick, G. M. (2008). *SADABS, Version 2008/1*. Göttingen: University of Göttingen.
- Shi, W., Wieder, B. J., Meyerheim, H. L., Sun, Y., Zhang, Y., Li, Y., Shen, L., Qi, Y., Yang, L., Jena, J., Werner, P., Koepf, K., Parkin, S., Chen, Y., Felser, C., Bernevig, B. A. & Wang, Z. (2021). *Nat. Phys.* **17**(3), 381–387.
- Shimomura, S., Hayashi, C., Asaka, G., Wakabayashi, N., Mizumaki, M. & Onodera, H. (2009). *Phys. Rev. Lett.* **102**, 076404.
- Shimomura, S., Hayashi, C., Hanasaki, N., Ohnuma, K., Kobayashi, Y., Nakao, H., Mizumaki, M. & Onodera, H. (2016). *Phys. Rev. B*, **93**, 165108.
- Shimomura, S., Murao, H., Tsutsui, S., Nakao, H., Nakamura, A., Hedo, M., Nakama, T. & Onuki, Y. (2019). *J. Phys. Soc. Jpn.* **88**(1), 014602.
- Stavinoha, M., Cooley, J. A., Minasian, S. G., McQueen, T. M., Kauzlarich, S. M., Huang, C. L. & Morosan, E. (2018). *Phys. Rev. B*, **97**(19), 195146.
- Stokes, H. T., Campbell, B. J. & van Smaalen, S. (2011). *Acta Crystallogr. A*, **67**, 45–55.
- Tomić, S., Biljaković, K., Djurek, D., Cooper, J., Monceau, P. & Meerschaut, A. (1981). *Solid State Commun.* **38**, 109–112.
- Wang, K., Mori, R., Wang, Z., Wang, L., Ma, J. H. S., Latzke, D. W., Graf, D. E., Denlinger, J. D., Campbell, D., Bernevig, B. A., Lanzara, A. & Paglione, J. (2021). *npj Quantum Mater.* **6**, 28.
- Wernick, J. H., Williams, H. J. & Gossard, A. C. (1967). *J. Phys. Chem. Solids*, **28**(2), 271–273.
- Wölfel, A., Li, L., Shimomura, S., Onodera, H. & van Smaalen, S. (2010). *Phys. Rev. B*, **82**, 054120.
- Zhu, X., Cao, Y., Zhang, J., Plummer, E. W. & Guo, J. (2015). *Proc. Natl. Acad. Sci. U. S. A.* **112**(8), 2367–2371.
- Zhu, X., Guo, J., Zhang, J. & Plummer, E. W. (2017). *Adv. Phys. X*, **2**(3), 622–640.
- Zhu, X. Y., Zhang, H., Gawryluk, D. J., Zhen, Z. X., Yu, B. C., Ju, S. L., Xie, W., Jiang, D. M., Cheng, W. J., Xu, Y., Shi, M., Pomjakushina, E., Zhan, Q. F., Shiroka, T. & Shang, T. (2022). *Physical Review B*, **105**(1), 014423.

Table 1. *Crystallographic data of crystal A of EuAl₄ at 250 K, 70 K and 20 K. Refinement method used: Least-squares on F. The superspace group (SSG; No.) is given according to*

Temperature (K)	<i>Stokes et al. (2011).</i>		
	250	70	20
Crystal system	Tetragonal	Orthorhombic	Orthorhombic
Space group; SSG	<i>I4/mmm</i>	<i>Fmmm(00σ)s00</i>	<i>Fmmm(00σ)s00</i>
No.	139	69.1.17.2	69.1.17.2
<i>a</i> (Å)	4.3949(1)	6.1992(4)	6.1991(3)
<i>b</i> (Å)	4.3949	6.2001(4)	6.1987(4)
<i>c</i> (Å)	11.1607(3)	11.1477(3)	11.1488(4)
Volume (Å ³)	215.57(1)	428.47(4)	428.41(4)
Wavevector, <i>q_z</i>	-	0.1781(3)	0.1741(2)
<i>Z</i>	2	4	4
Wavelength (Å)	0.50000	0.50000	0.50000
Detector distance (mm)	110	260	260
2θ-offset (deg)	0	0, 25	0, 25
χ-offset (deg)	-60	-60	-60
Rotation per image (deg)	1	1	1
(sin(θ)/λ) _{max} (Å ⁻¹)	0.682610	0.748910	0.749031
Absorption, μ (mm ⁻¹)	5.8373	5.9090	5.9100
T _{min} , T _{max}	0.3211, 0.3712	0.3209, 0.3732	0.3192, 0.3676
Criterion of observability	<i>I</i> > 3σ(<i>I</i>)	<i>I</i> > 3σ(<i>I</i>)	<i>I</i> > 3σ(<i>I</i>)
Number of main reflections			
measured	1407	473	470
unique (obs/all)	109/109	174/174	176/176
Number of satellites			
measured	-	929	928
unique (obs/all)	-	279/316	263/322
<i>R</i> _{int} main (obs/all)	0.0374/0.0374	0.0136/0.0136	0.0188/0.0188
<i>R</i> _{int} sat (obs/all)	-	0.0581/0.0588	0.0606/0.0616
No. of parameters	9	18	18
<i>R_F</i> main (obs)	0.0147	0.0165	0.0213
<i>R_F</i> sat (obs)	-	0.0369	0.0311
<i>wR_F</i> main (all)	0.0214	0.0203	0.0230
<i>wR_F</i> sat (all)	-	0.0395	0.0336
<i>wR_F</i> all (all)	0.0214	0.0245	0.0250
GoF (obs/all)	1.53/1.53	1.13/1.09	0.93/0.88
Δρ _{min} , Δρ _{max} (e Å ⁻³)	-1.35, 1.15	-2.40, 3.58	-1.49, 1.58

Table 2. *Crystallographic data for three models for the modulated crystal structure at 70 K, based on different superspace groups. Criterion of observability: $I > 3\sigma(I)$*

Model	A	B	C
a (Å)	4.3834(3)	4.3835(3)	6.1992(4)
b (Å)	4.3834	4.3841(3)	6.2001(4)
c (Å)	11.1488(4)	11.1475(3)	11.1477(3)
V (Å ³)	214.21(2)	214.23(2)	428.47(4)
\mathbf{q}	0.1782(3) \mathbf{c}^*	0.1781(3) \mathbf{c}^*	0.1781(3) \mathbf{c}^*
SSG	$I4/mmm(00\sigma)0000$	$Immm(00\sigma)s00$	$Fmmm(00\sigma)s00$
R_{int} main (obs/all)%	1.53/1.53	1.28/1.28	1.36/1.36
R_{int} sat (obs/all)%	7.43/7.49	6.75/6.85	5.81/5.88
R_F main (obs/all)%	4.37/4.37	1.96/1.96	1.65/1.65
R_F sat (obs/all)%	60.46/70.53	5.25/5.83	3.69/4.05
Unique main (obs/all)	130/130	225/225	174/174
Unique sat (obs/all)	215/254	365/425	279/316
No. of parameters	13	19	18

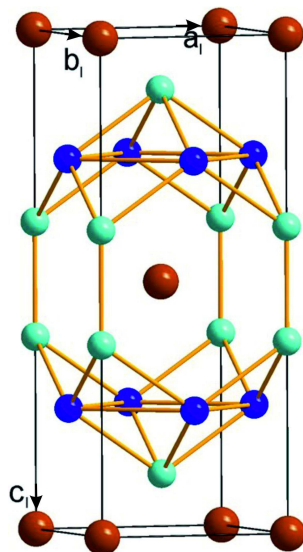


Fig. 1. Crystal structure of EuAl_4 with space group $I4/mmm$ in the periodic phase at 250K. Depicted is the I -centered unit cell with basis vectors \mathbf{a}_I , \mathbf{b}_I and \mathbf{c}_I . Brown spheres correspond to the Eu atoms; dark blue spheres represent Al1 atoms; and green spheres stand for Al2 atoms. Shortest interatomic distances are: $d[\text{Eu}-\text{Eu}] = 4.3949(2)$ Å, $d[\text{Al1}-\text{Al1}] = 3.1077(1)$ Å, $d[\text{Al2}-\text{Al1}] = 2.664(1)$ Å and $d[\text{Al2}-\text{Al2}] = 2.568(4)$ Å.

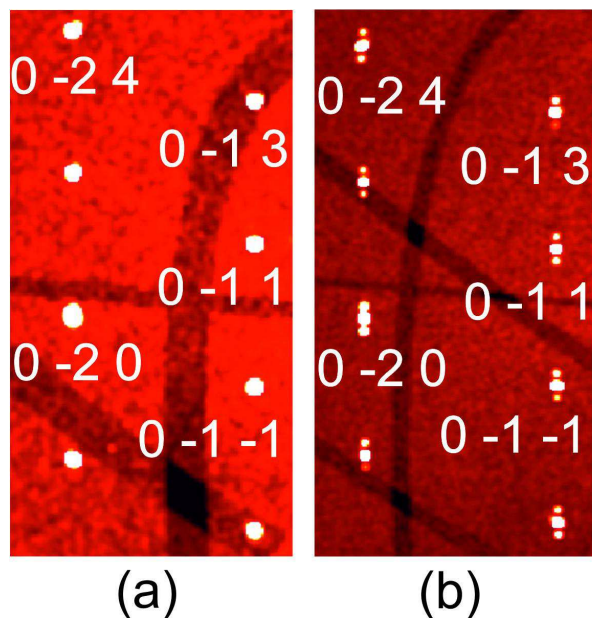


Fig. 2. Excerpt of the reconstructed reciprocal layer ($0kl$) for SXRD data measured at (a) $T = 250$ K, and (b) 70 K. Indices are given for several main reflections. Panel (b) is better resolved than panel (a), because of the longer crystal-to-detector distance at 70 K. Dark bands are due to insensitive pixels between the active modules of the PILATUS3 X CdTe 1M detector.

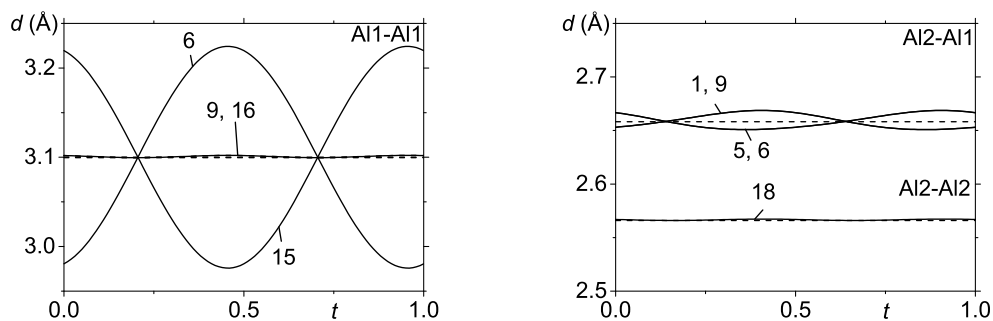


Fig. 3. t -Plot of interatomic distances (\AA) $d[\text{Al1-Al1}]$, $d[\text{Al2-Al1}]$ and $d[\text{Al2-Al2}]$ at 70 K, where the first atom is the central atom. The number on each curve is the number of the symmetry operator that is applied to the second atom of the bond pair. Symmetry operators are listed in Table S5 in the supporting information.

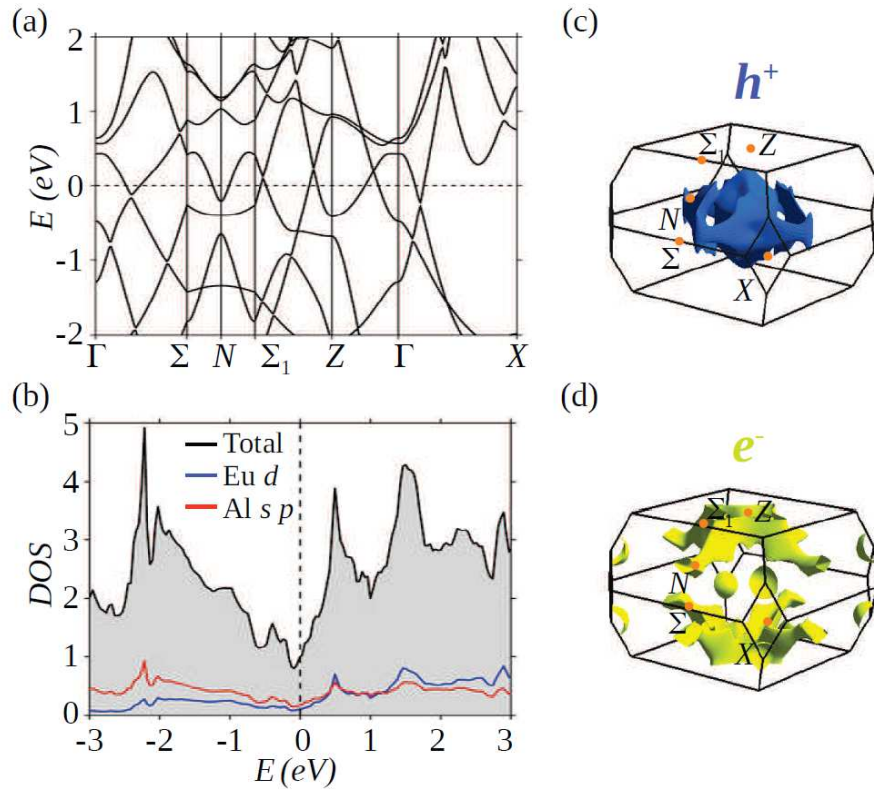


Fig. 4. (a) Bulk band structure and (b) Density-of-states (DOS) of EuAl_4 . The dashed lines in (a) and (b) mark the Fermi level at energy (E) zero. The calculated (c) hole (blue) and (d) electron (yellow) Fermi pockets in the primitive bulk Brillouin zone. Three-dimensionally (3D) structured hole and electron Fermi pockets are resolved.

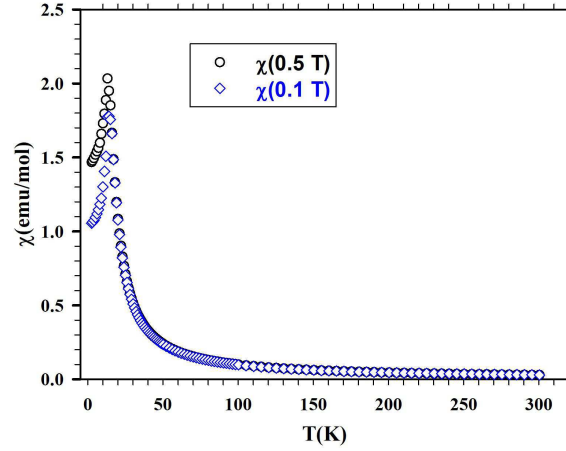


Fig. 5. Temperature dependent magnetic susceptibility of EuAl_4 from 2.4 to 300 K. Data measured in fields of 0.1 T and 0.5 T.

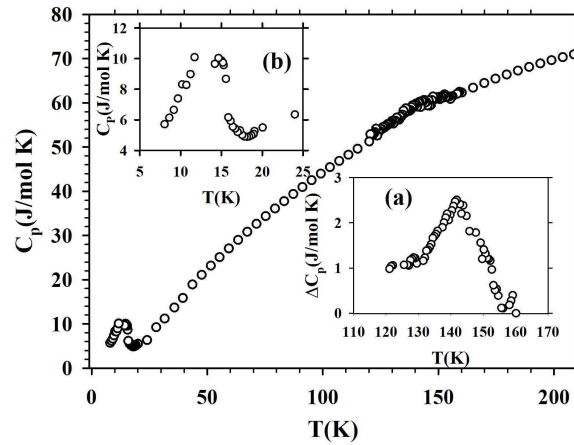


Fig. 6. Temperature dependence of the specific heat C_p from 8 to 210 K. The lower inset (a) provides an enlarged view around the anomaly at 145 K, where $\Delta C = 2.5$ J/(mol K). The upper inset (b) displays C_p vs T at low temperatures 8–25 K.

Synopsis

The incommensurate charge-density-wave of EuAl_4 below $T_{CDW} = 145$ K is found to possess orthorhombic symmetry, despite an average crystal structure that remains tetragonal in very good approximation. This finding has ramifications for the interpretation of all physical properties of EuAl_4 , in particular its multiple magnetic transitions.
